Oxidation of Metals, Vol. 61, Nos. 3/4, April 2004 (© 2004)

Thermal Conductivity, Phase Stability, and Oxidation Resistance of $Y_3Al_5O_{12}$ (YAG)/Y_2O_3–ZrO_2 (YSZ) Thermal-Barrier Coatings

Y. J. Su,*† R. W. Trice,#† K. T. Faber,†$ H. Wang,‡ and W. D. Porter‡

Received January 13, 2003; revised January 14, 2004

This paper describes a new multilayer TBC that incorporates a 10 μm-thick oxygen barrier layer of yttrium–aluminum garnet (YAG) into a typical YSZ TBC system. The thermal conductivity of as-sprayed YAG/YSZ coatings was reduced due to excessive porosity and amorphous areas in the YAG layer. After long-term heat treatments, the conductivity of the multilayer was unaffected by the presence of YAG. Sintering and recrystallization of the amorphous YAG regions occurred during high-temperature heat treatments. While YAG itself possesses excellent phase stability, its presence also improved the phase stability of zirconia near the YAG/YSZ interface, inhibiting the outward diffusion of yttrium from high-yttria t-ZrO_2 The YAG layer reduced the NiCoCrAlY bond-coat oxidation rate by a factor of three during isothermalfurnace tests conducted at 1200°C.

KEY WORDS: thermal barrier coating; conductivity; X-ray diffraction; garnet; zirconia.

INTRODUCTION

Thermal-barrier coatings (TBCs) have been used to protect gas-turbine-engine components since the 1970s. The state-of-the-art yttria partially stabilized zirconia (YSZ) TBCs are effective in reducing heat transfer to the

†Department of Materials Science and Engineering, Northwestern University, Evanston, IL, USA.
‡Metals and Ceramics Division, Oak Ridge National Laboratory, Oak Ridge, TN, USA.
*Present address. General Electric Co., Global Research Center, Schenectady, NY, USA.
#Present address. School of Materials Engineering, Purdue University, West Lafayette, IN, USA.
$To whom correspondence should be sent. e-mail: k-faber@northwestern.edu

0030-770X/04/0400–0253/0

underlying substrate. However, ultimately, their lifetime is limited by the combination of the applied loading of the TBC system in concert with microstructural and chemical changes which occur at elevated temperatures. Although chemical changes in the bond coat and sintering and loss of strain tolerance in the top coat contribute to failure, TBC failure typically is related to stresses (growth and thermal) associated with the formation of a thermally grown oxide (TGO) at the bond coat/top coat interface.[1,2] Various approaches have been taken to improve the oxidation resistance of TBCs. Sun *et al.*[3] and Tsui and Clyne[4] have explored the use of alumina oxygen-barrier layers. Although they report an improvement in oxidation resistance, there are two downfalls to using plasma-sprayed Al_2O_3 which deposits as γ-Al_2O_3. First, γ-Al_2O_3 is unstable with respect to long-term, high-temperature exposure as it transforms to δ-Al_2O_3 and then to α-Al_2O_3.[5] The accompanying 11 vol.% reduction can produce undesirable stresses. Second, the thermal conductivity of Al_2O_3 (5.3 W/m K)[6] is significantly higher than that of YSZ (2.0 W/m K)[7] at $\sim$1100°C.

This paper explores a multilayer coating with the potential to improve oxidation resistance while maintaining low thermal conductivity and good phase stability. Padture and Klemens[8] first proposed yttrium–aluminum garnet ($Y_3Al_5O_{12}$ or YAG) as a potential thermal barrier coating material. As shown in Table I, bulk YAG has an excellent low oxygen diffusivity and a reasonably low thermal conductivity that is only slightly higher than that of YSZ. Specifically, a small-particle plasma-sprayed coating consisting of a thin layer of YAG coupled with a thicker layer of 7 wt.% Y_2O_3–ZrO_2 (YSZ) is proposed. The objective of this work is to quantify the effect of YAG on thermal resistance, long-term phase stability, and oxidation resistance of a multilayer YAG/YSZ coating.

EXPERIMENTAL PROCEDURES

Small-Particle Plasma-Spray Processing

Small-particle plasma spray (SPPS) is a modified air plasma spray method that incorporates a unique angled powder injector.[9] The injector

Table I. Relevant Material Properties of Fully Dense, Bulk YAG and YSZ

Dense, bulk material	Thermal conductivity (W/m K)	Oxygen diffusivity (m^2/s)
Y_2O_3–ZrO_2 (YSZ)	2 (1127°C)	10^{-10}–10^{-11}
$Y_3Al_5O_{12}$ (YAG)	3.2 (1000°C)	10^{-25} (volume) 10^{-20} (grain boundary)

Table II. Plasma-gun Condition Used to Deposit the YSZ and YAG Coatings

Spray parameter	YSZ	YAG
Power (kW)	35	50
Voltage (V)	60	67
Current (A)	583	745
Argon primary gas flow (slm)	32	32
Hydrogen secondary gas flow (slm)	8	13
Spray distance (cm)	6	6
Argon carrier gas flow (slm)	5	5

geometry has been previously described.[10] An external transverse injection Plasma-Technik F-4 gun with a 6 mm nozzle and an Ar/H_2 gas mixture, along with a Plasma-Technik Twin 10 powder feeder was used to prepare all samples. A constant set of gun conditions was used for each powder (Table II). The angular YSZ[†] powder, formed by a fusing and crushing process, possesses a mean particle size of $11.9 \pm 0.2\,\mu$m. The as-received spherical YAG[‡] powder, formed by combustion-spray pyrolysis, has a mean particle size of $23.0 \pm 0.2\ \mu$m. It was modified by dry ball-milling to reduce the average particle size to $18.1 \pm 0.7\ \mu$m.

The thermal conductivity and phase-stability samples consisted of a 10 μm thick layer of YAG embedded between a 30 and 200 μm-thick layer of YSZ, as shown schematically in Fig. 1a. For comparison, coatings of pure YSZ were also produced. Both sets were made by depositing the plasma-sprayed coating onto aluminum-coated steel. The aluminum layer was etched away in dilute hydrochloric acid (10–20 vol.% HCl) to obtain free-standing coatings for testing. Oxidation samples were prepared as follows: Disk-shaped samples of bare and bond-coated Inconel 939 substrates were machined by Electrical-Discharge Machining (EDM) to a nominal sample diameter of 1.91 ± 0.003 cm prior to spraying the ceramic coatings. A low-pressure plasma-sprayed NiCoCrAlY bond coat $\sim$150 μm thick had previously been applied to the top face of some of the samples. A proprietary diffusion-bonding heat treatment was conducted after bond coat deposition by Siemens-Westinghouse. The oxidation samples contained a 10 μm-thick layer of YAG above an 80 μm-thick layer of YSZ, as shown schematically in Fig. 1b.

Thermal Conductivity Measurements

Thermal-diffusivity measurements of free-standing coatings were made using the laser flash technique first developed by Parker *et al.*[11]

[†]Amperit 825.0, H. C. Stark Inc., Newton, MA, USA.
[‡]Y_3Al_5 Oxide, Praxair Specialty Ceramics, Woodinville, WA, USA.

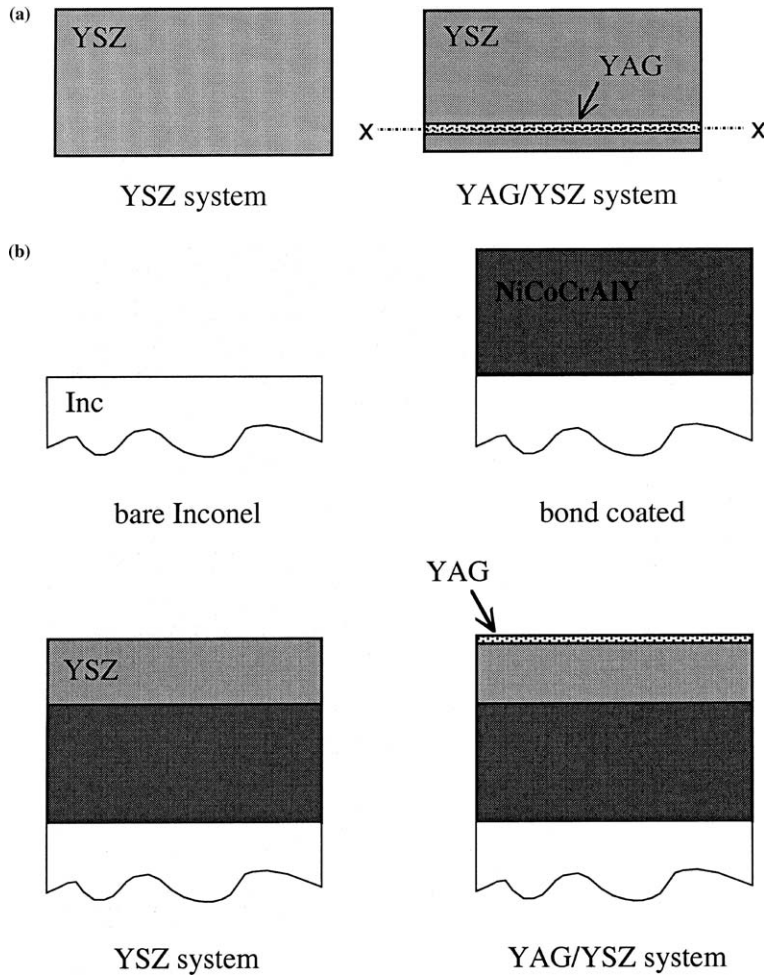

Fig. 1. Schematic drawings of (a) thermal-conductivity and phase-stability samples, and (b) oxidation samples.

All measurements were conducted at Oak Ridge National Laboratory in the High Temperature Materials Laboratory. A detailed description of the laser flash system has been discussed previously.[12] Samples were disk-shaped measuring ~12.5 mm in diameter. Coating thickness was measured using a micrometer prior to testing. Six samples were tested concurrently, and three measurements were taken and averaged for each specimen at each temperature. One replicate was run for each sample.

Specific heat was measured using a differential scanning calorimeter (Stanton Redcroft DSC1500) with a sapphire standard. Sample disks 4 mm in diameter were stacked to obtain a weight of approximately 90 mg. The heat flow was measured from 25 to 1000°C with a 20°C/min ramp rate. All samples were heat treated for 1 hr at 1000°C in air prior to the measurement because some as-sprayed samples produced unstable exothermic reactions around 900°C. A best-fit line of specific heat vs. temperature data was extrapolated to obtain values between 1100 and 1200°C.

The Archimedes' technique was used to measure coating bulk density and total porosity.[13] Three measurements were taken and averaged for each coating. Thermal conductivity, k, was then calculated using the following equation:

$$k = \alpha(T)C_p(T)\rho \tag{1}$$

where α is thermal diffusivity, C_p is specific heat, both of which are a function of temperature, T, and ρ is bulk density. The conductivity of as-sprayed and aged coatings was determined. Aging was conducted at 1200°C for 50 and 100 hr. Based on the error associated with the three individual factors, the total error associated with the full set of measurements was estimated to be approximately 6%.

Phase Stability Experiments

To study coating behavior near service temperatures, free-standing specimens were exposed to various heat treatments in static air. Coatings were heated for 100 hr at 1200 and 1300°C with a 10°C/min ramp rate. X-ray powder diffraction was performed on as-sprayed and heat-treated coatings to investigate large-scale effects of zirconia destabilization. Aluminum was added to the powders as an internal standard. X-ray diffraction of intact YAG/YSZ coatings was used to study local effects of the YAG on the YSZ phase stability. All X-ray studies were performed using a Scintag diffractometer with CuK_α radiation. A slow scan over 72–76°C 2θ with a 0.01° step and 50 s count time was conducted to monitor the (400) cubic (c) and tetragonal (t) zirconia peaks. Peaks were fit using the default-parabolic-fit routine, "Digital Filtering" within the "Peak Finder" function (Scintag, DMSNT Ver 1.37).

Intact YAG/YSZ heat-treated coatings were split at the interface between the YAG and YSZ (along X in Fig. 1a) with a razor blade in order to expose surfaces appropriate for the study of local changes in phase stability. The back face of the pure YSZ coatings was tested for comparison. The samples were oriented with the beam aimed at the exposed YAG surface, assumed to be $\sim$5 μm thick (half of the original

layer thickness). Given the limited effective X-ray penetration depth, signal is detected from the exposed YAG and a portion of the zirconia that is beneath it. The maximum effective X-ray penetration depth can be determined by considering pure zirconia and pure YAG. The penetration depth in pure zirconia and pure YAG (for 99% of the integrated X-ray intensity) was determined to be ~6 and 12 μm, respectively.[14] The actual effective penetration depth in the zirconia layer is less than 6 μm because some of the signal is attenuated in the top YAG layer. In other words, only YAG and a near-interface layer of zirconia a few microns thick contributes to the X-ray pattern of the YAG/YSZ coatings.

Oxidation Tests

A tube furnace was used to conduct isothermal tests at 1200°C for 1, 12.5, and 50 hr in static air with a 10°C/min ramp rate. Four types of samples were tested with 1–3 replicates of each: (a) bare Inconel, denoted Inc, (b) NiCo-CrAlY bond-coated Inconel, denoted BC, (c) YSZ/NiCo-CrAlY/Inc, denoted YSZ system, and (d) YAG/YSZ/NiCoCrAlY/Inc, denoted YAG/YSZ system YG, all shown schematically in Fig. 1b. The coatings were sprayed directly on the top face of the samples with ~1 mm of overspray on the sides, covering the entire bond coat. The side overspray was of poorer quality compared to that on the top surface. Since coatings were applied only to the top face of the samples, the bare Inconel sample was tested in order to isolate the weight gain due only to bond-coat oxidation on the top face by establishing a baseline oxidation rate of the side and bottom surface. Inconel actively oxidizes at high-temperature which causes catastrophic TGO flaking on the surface. These oxide flakes must be contained to conduct quantitative weight gain measurements. Thus, all of the samples were wrapped loosely in platinum foil to contain any spalled oxide, but were exposed enough to permit adequate air flow. The effect of the platinum foil on weight change measurements was checked by heating the foil alone under identical oxidation conditions. No weight gain occurred in these experiments, nor was any PtO_2 detected by EDX in the TBC systems.

Weight gain was determined by weighing the Pt-wrapped samples prior to testing and after high-temperature exposure and cooling to room temperature. Based upon the earlier TBC studies,[15–18] parabolic kinetics were assumed to govern the oxidation behavior of these materials.[§] The parabolic rate constant was determined using

[§]Sub-parabolic oxidation kinetics have been observed in some Ni-containing alloys,[19,20] but only after a long time, beyond those examined in this study.

$$\Delta w/A = k_p^{1/2} t^{1/2} \tag{2}$$

where Δw is the weight gain, A is the surface area, k_p is the oxidation rate constant, and t is the exposure time. The weight gain on the top face due to bond-coat oxidation was determined from the weight gain of the total surface and the specific weight gain for the bare Inconel sample. The following equation was used to subtract out the effect of the exposed Inconel surface on the coated specimens:

$$[\Delta w/A]_{\text{top}} = \{\Delta w_{\text{Total}} - ([\Delta w/A]_{\text{Inc}} \times [A_{\text{side}} + A_{\text{bottom}}])\}/A_{\text{top}} \tag{3}$$

where the subscripts "top," "side," and "bottom" refer to the various surfaces. The specific weight gain for the Inconel surface, $[\Delta w/A]_{\text{Inc}}$, was based on the total surface area of the uncoated Inconel sample.

RESULTS AND DISCUSSION

Coating Microstructure

An SEM cross-sectional micrograph of the YAG/YSZ multilayer coating is shown in Fig. 2. TEM analysis reveals classic columnar structures in the YSZ (Fig. 3a) but an excessive amount of submicron porosity in the

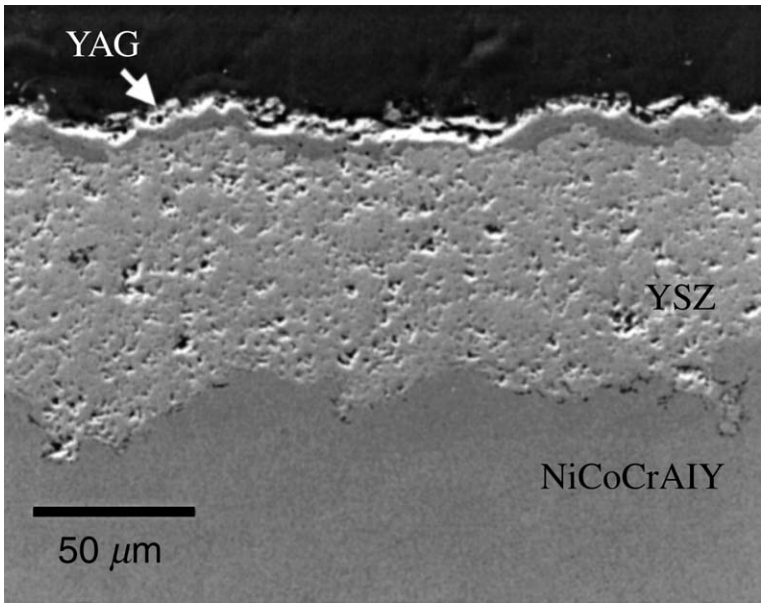

Fig. 2. SEM micrograph of as-sprayed YAG/YSZ coating.

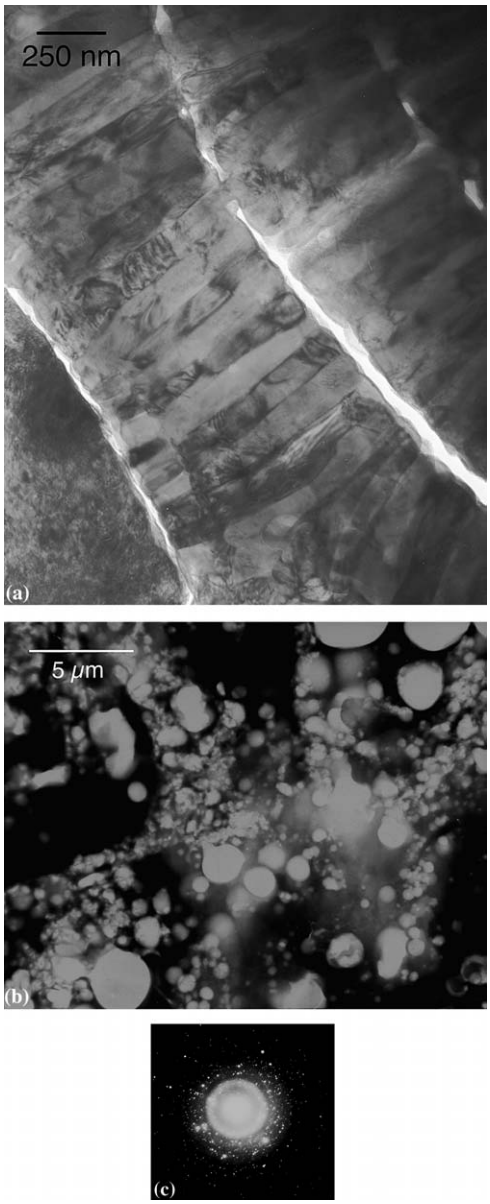

Fig. 3. TEM micrograph of as-sprayed coatings: (a) pure YSZ and (b) YAG/YSZ coating. Excessive porosity in the YAG coating, compared to the typical YSZ coating, is apparent. Electron-diffraction pattern in (c) reveals both amorphous and crystalline regions.

YAG layer (Fig. 3b). The YAG layer in the multilayer coating has significantly more porosity than a traditional plasma-sprayed coating. Electron-diffraction analysis (Fig. 3c) indicates that both amorphous and crystalline regions are present in the YAG.

Thermal Conductivity

As-Sprayed Coatings

The conductivity of as-sprayed pure YSZ coatings and YAG/YSZ multilayer coatings is shown in Fig. 4. Previous experiments on Al_2O_3/YSZ multilayers[5,21,22] established that a series rule-of-mixtures model explains the conductivity, k, of a multilayer coating:

$$k = k_1 k_2 / (v_1 k_2 + v_2 k_1) \tag{4}$$

where v represents volume fraction of each phase and the subscripts 1 and 2 refer to the phase. The model prediction, plotted in the same figure, is determined using experimental values obtained for the YSZ coating and published bulk values for the YAG. The volume fraction of YAG was measured and averaged using image analysis on five SEM images. The experimental multilayer values measured from 400 to 1200°C are 20% lower than the predicted value. The low multilayer conductivity value can

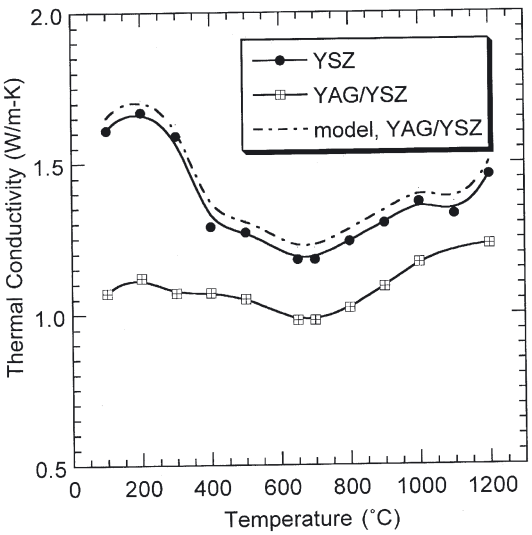

Fig. 4. Thermal conductivity of as-sprayed YSZ and YAG/YSZ coatings, plotted with a series model prediction for the multilayer coating.

be correlated to the two microstructural features described above. One is the additional submicron porosity present in the YAG layer, as revealed in the TEM micrograph shown in Fig. 3b. Previous studies on YSZ demonstrated that thermal conductivity is very sensitive to small changes in density. Trice *et al.* showed that a ~5% decrease in density can result in a ~22% decrease in conductivity.[23] Thus, the porosity in the YAG layer contributes to lowering the overall thermal conductivity of the multilayer coating.

The remaining decrease in conductivity is likely due to the amorphous content of the YAG coating. Studies on diamond-like carbon thin films[24] and boron carbide[25] have shown that an amorphous material can have a significantly lower thermal conductivity than its crystalline counterpart. This is due to the random energy transfer that occurs in the "disordered" atomic arrangement that exists in an amorphous structure.[24]

Aged Coatings

Conductivity values for aged coatings are shown in Fig. 5 for the pure and multilayer coatings. After 50 hr at 1200°C, the conductivity of the pure coating has risen only 15%, whereas the multilayer conductivity (measured at 1200°C) has increased by 50%. Sintering and the subsequent reduction of porosity and microcracks, certainly contributes to the rising conductivity in both coatings. Furthermore, it is likely that the amorphous regions in the YAG layer crystallized within the first 50 hr, resulting in a more rapid initial increase in conductivity.

Phase Stability

The powder X-ray diffraction patterns for the as-received YAG powder, as-sprayed coating, and heat-treated coating are shown in Fig. 6. All the peaks in the as-sprayed pattern correspond to YAG or the internal aluminum standard; the cubic YAG phase is maintained during the spraying process (Fig. 6a) as well as after heat treatment (Fig. 6b). This extensive phase stability is an advantage that YAG possesses as an oxygen-barrier material over Al_2O_3 which undergoes various crystallographic transformations described in the introduction.

The results for as-sprayed YSZ coatings are presented in Fig. 7a. Zirconia is present as non-equilibrium t-ZrO_2 in both coatings. Non-equilibrium t-ZrO_2 contains a higher percentage of Y_2O_3 (~7 wt.%) than the equilibrium t-ZrO_2 (4 wt.%); they are often referred to as high-yttria and low-yttria tetragonal phases, respectively.[26] Cubic zirconia also forms with a higher amount of Y_2O_3 (~14 wt.%), making it a stable phase at low temperatures. Thus, the transformation from high-yttria t-ZrO_2 to

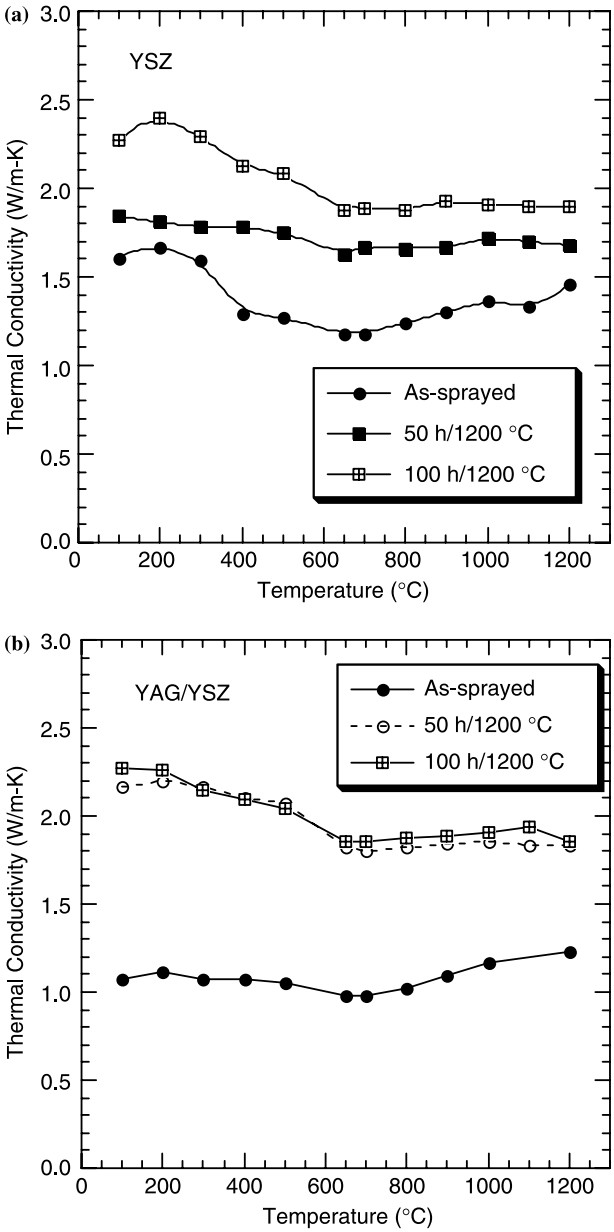

Fig. 5. Thermal conductivity of aged coatings: (a) YSZ and (b) YAG/YSZ.

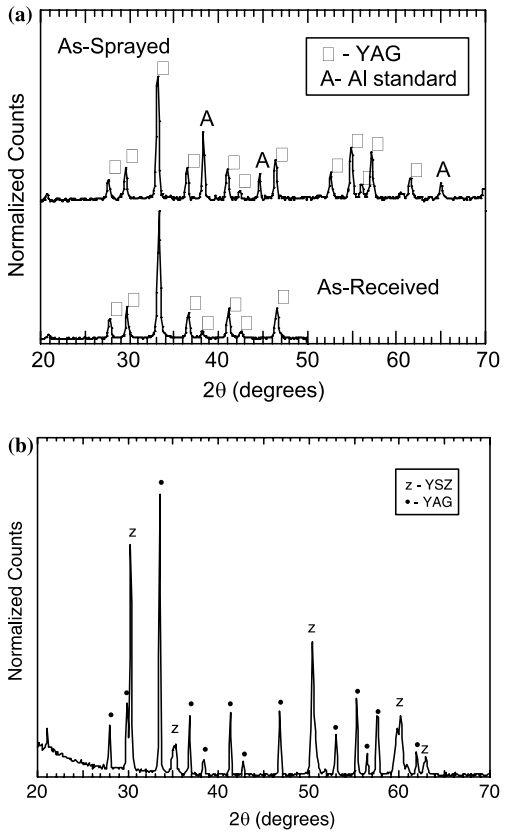

Fig. 6. X-ray diffraction results for (a) as-received and as-sprayed YAG indicating stability during spraying and (b) YAG/YSZ coating heat-treated for 100 hr at 1200°C showing good YAG phase stability after long-term exposure.

low-yttria *t*- and *c*-ZrO_2 requires the diffusion and redistribution of yttrium cations. Results for the heat-treated coatings are shown in Fig. 7b and c and Fig. 8a and b and show evidence for such redistribution. There is a distinct difference between the YSZ and the YAG/YSZ in the transition from high-yttria *t*-ZrO_2 after 100 hr at both 1200 and 1300°C. Diffusion of yttrium from the near-interface zirconia in the multilayer coating is inhibited, as evidenced by the non-equilibrium diffraction peak. High-yttria *t*-ZrO_2 in the YSZ coating completely transforms to low-yttria *t*-ZrO_2 and *c*-ZrO_2 after the 1300°C heat treatment, whereas a residual amount of high-yttria *t*-ZrO_2 still exists in the multilayer coating.

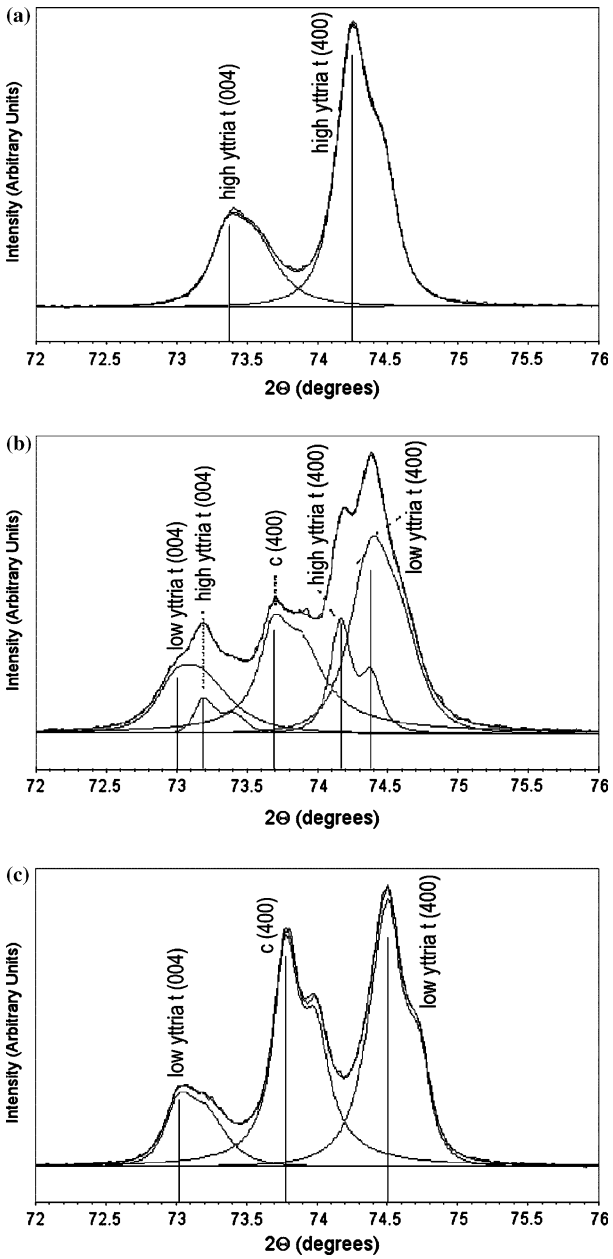

Fig. 7. X-ray diffraction results for YSZ coatings: (a) as-sprayed, (b) 100 hr at 1200°C, and (c) 100 hr at 1300°C.

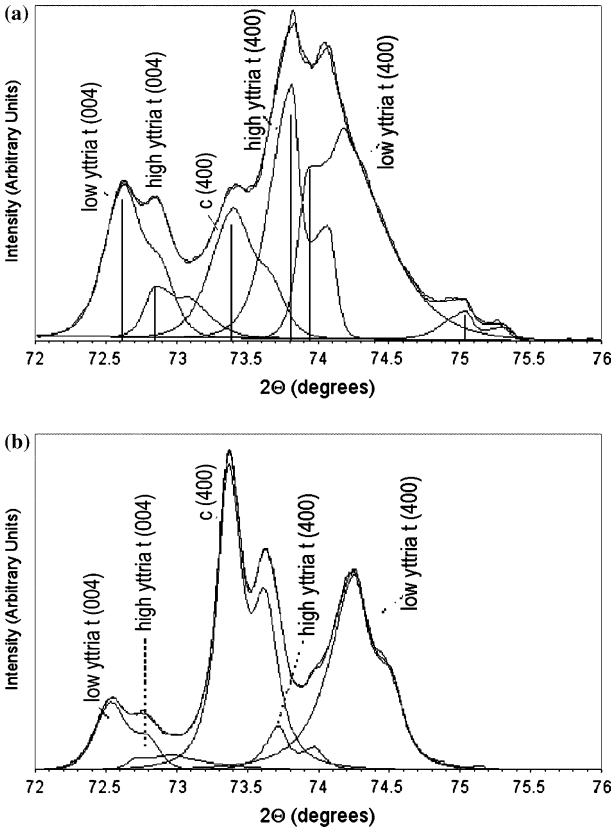

Fig. 8. X-ray diffraction results for YAG/YSZ coatings: (a) 100 hr at 1200°C and (b) 100 hr at 1300°C.

The presence of YAG may influence the phase stability of high-yttria t-ZrO_2 in the near-interface zirconia region by increasing the local yttria chemical potential. It is plausible that the neighboring layer of YAG raises the local activity of yttrium due to interdiffusion, affording greater stability to the high-yttria t-ZrO_2 at the temperatures studied. This phenomenon of phase stability in layered microstructures has largely been explored in the investigation of multilayer thin films.[27]

Oxidation Resistance

Microstructural and Phase Analyses

SEM micrographs of the TGO in the as-sprayed and oxidized microstructures of the YSZ system are shown in Fig. 9. There are two distinct

regions in the TGO which is dense and continuous after 1 hr. Initially, discontinuous pockets of transient oxides develop; these are the lighter gray areas in the TGO as seen in Fig. 9. EDX analysis reveals the presence of Ni, Co, Cr, and Al in these locations whereas the darker continuous regions contain primarily Al. Identical observations were seen in the YAG/YSZ system, but with different TGO thicknesses.

X-ray diffraction reveals the presence of multiple phases in the TGO over time: primarily α-Al_2O_3, $NiAl_2O_4$, and $CoAl_2O_4$ spinels, with smaller amounts of NiO. All of these phases appear after only 1 hr. Furthermore, after 12.5 hr at 1200°C, YAG is also detected on the bare bond-coat surface. These phases are commonly observed in similar bond-coat systems.[15,16,18,28] Although some studies have noted the presence of $YAlO_3$[17] and θ-Al_2O_3,[29] these phases were not observed in this, nor other investigations.[15,18] The initial formation of an inner continuous layer of α-Al_2O_3 is consistent with the relative standard free energy of formation of the various TGO phases, with α-Al_2O_3 possessing the lowest Gibbs free energy of formation.[30] In other words, it is more energetically favorable for α-Al_2O_3 rather than the secondary oxides, to form.

Rate Constant Determination

The specific weight gain of the top surface is shown vs. time and square root in Fig. 10. As expected in diffusion-limited oxidation, the weight gain is parabolic with respect to time. The samples rank in terms of decreasing weight gain at all oxidation times as: Inc, BC, YSZ system, YAG/YSZ system. No measurable weight change was detected with the platinum foil itself under all oxidation conditions used in this investigation. Values for the bond-coated sample are shown for 1 and 12.5 hr for comparison. Its weight gain is slightly higher than that for pure YSZ, indicating the YSZ does afford a minor amount of oxidation resistance, also noted by Wu *et al.*[15] and Brindley and Miller.[31] The slope of the linear fit in Fig. 10b is equal to the square root of the parabolic rate constant, k_p, based on Eq. 2. The rate constant, k_p, equals 1.88×10^{-4} mg^2/cm^4-s for the YSZ system and 6.56×10^{-5} mg^2/cm^4-s for the YAG/YSZ system. The R^2 value for the linear fit is 98.1% and 99.1% for the YSZ and YAG/YSZ systems, respectively. The presence of a thin layer of YAG reduces the rate constant by a factor of about three. YAG's low oxygen diffusivity (Table I) inhibits oxygen transport through the top coat, slowing down TGO formation on the bond-coat surface. Fully-dense YAG possesses an oxygen diffusivity that is 10 orders of magnitude lower than that of YSZ. However, despite YAG's relatively low diffusivity value, there is only a moderate reduction in the bond-coat oxidation rate. This is due to the high percentage of pores in SPPS YAG which serve as fast-oxygen-transport

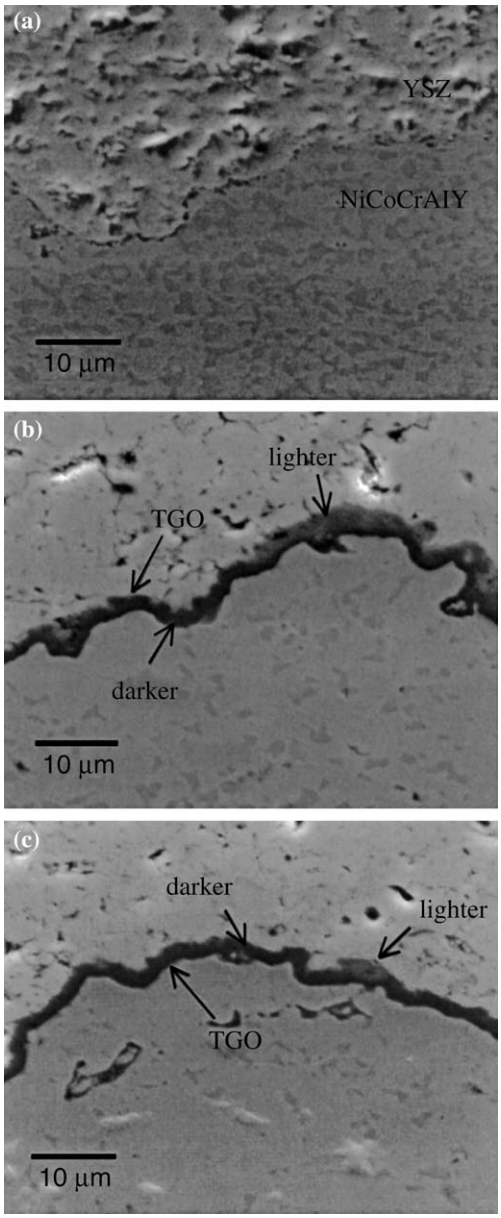

Fig. 9. SEM micrograph of: (a) as-sprayed coating, (b) YSZ system after 1 hr at 1200°C, and (c) YAG/YSZ system after 1 hr at 1200°C.

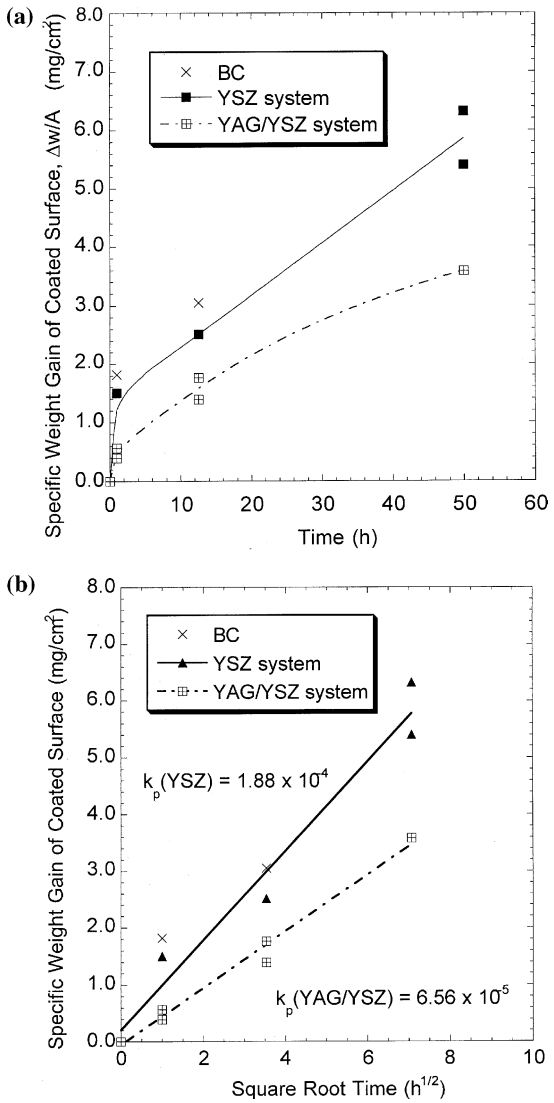

Fig. 10. Specific weight gain of coated surface plotted vs. (a) time and (b) square root time. The k_p values are given in units of mg^2/cm^{4-5}.

paths. It is also likely due to the poorer quality of the YAG overspray on the sides of the samples compared to the top surface, allowing oxygen ingress from the sides. This additional ingress caused delamination at the TGO/top coat interface after 50 hr.

SUMMARY

The feasibility of using SPPS to produce effective thin oxygen barrier layers has been demonstrated. The YAG/YSZ multilayer coatings exhibited enhanced heat resistance in the as-sprayed state due to additional porosity and amorphous regions. Although the conductivity did increase due to sintering, the presence of YAG did not detrimentally raise thermal conductivity beyond that of pure YSZ upon extended high-temperature exposure. Unlike other oxygen barrier materials that have been explored, e.g. Al_2O_3, YAG demonstrated good phase stability after long high-temperature exposure. Additionally, the presence of YAG improved the zirconia phase stability on a local scale, i.e. near the interface with YAG. Weight-gain measurements and SEM/EDX analysis reveal greater oxidation in the pure YSZ system for a given oxidation time and temperature. The presence of YAG improves the bond-coat oxidation resistance by a factor of $\sim$3, based on the parabolic rate constant. These findings suggest that multilayer YAG/YSZ coatings show promise for improved thermal-barrier protection.

ACKNOWLEDGMENTS

Funding was provided by the U.S. Department of Energy, Federal Energy Technology Center, Cooperative Agreement No. DE-FC21-92MC 29061, under subcontract 96-01-SR047. The thermal conductivity testing was supported by the U.S. DOE, Assistant Secretary of Transportation Technologies, as part of the HTML User Program under contract DE-AC05-00OR22725, managed by UT-Batelle, LLC. The authors would like to thank Richard Marzec for general assistance in the thermal spray laboratory. Discussions with Dr. Thomas Bernecki were also very useful. The assistance of Dr. Ramesh Subramanian at Siemens-Westinghouse in obtaining superalloy substrates is also appreciated.

REFERENCES

1. P. K. Wright and A. G. Evans, *Current Opinion in Solid State and Materials Science* **4**, 255–265 (1999).
2. A. Rabiei and A. G. Evans, *Acta Materialia*, **48**, 3963–3976 (2000).
3. J. H. Sun, E. Chang, C. H. Chao and M. J. Cheng, *Oxidation of Metals*, **40**, 465 (1993).
4. Y. C. Tsui and T. W. Clyne, in *Thermal Spray: Practical Solutions for Engineering Problems*, C. C. Berndt, ed. (ASM International, Materials Park, OH, 1996), pp. 275–284.
5. Y. J. Su, H. Wang, W. D. Porter, A. R. de Arellano Lopez and K. T. Faber, *Journal of Materials Science* **36**, 3511 (2001).
6. W. D. Kingery, H. K. Bowen and D. R. Uhlmann, *Introduction to Ceramics, 2nd ed.* (John Wiley & Sons, New York, 1976), p. 620.

7. D. P. H. Hasselman, L. F. Johnson, L. D. Bentsen *et al.*, *American Ceramic Society Bulletin* **66**, 799 (1987).
8. N. P. Padture and P. G. Klemens, *Journal of American Ceramic Society* **80**, 1018 (1997).
9. T. F. Bernecki and D. R. Marron, *Small Particle Plasma Spray Apparatus, Methods, and Coated Article.* U.S. Patent No. 5 744 777 and No. 5 858 470, Northwestern University, Evanston, IL (1998, 1999).
10. Y. J. Su, T. F. Bernecki and K. T. Faber, *Journal of Thermal Spray Technology* **11**, 52 (2002).
11. W. J. Parker, R. J. Jenkins, C. P. Butler and G. L. Abbott, *Journal of Applied Physics* **32**, 1679 (1961).
12. H. Wang, R. B. Dinwiddie and P. S. Gaal, in *Thermal Conductivity 23*, K. E. Wilkes, R. B. Dinwiddie and R. S. Graves, eds. (Technomic Publishing Co., Lancaster, PA, 1996), pp. 119–126.
13. ASTM C373–88 (ASTM International, West Conshohocken, PA, 1999).
14. B. D. Cullity, *Elements of X-ray Diffraction* (Addison-Wesley Publishing Company, Reading, MA, 1978).
15. B. C. Wu, E. Chang, D. Tu and S. L. Wang, *Materials Science and Engineering A* **111**, 201 (1989).
16. W. Brandl, *Surface and Coatings Technology* **86–87**, 41 (1996).
17. N. Czech, M. Juez-Lorenzo, V. Kolarik and W. Stamm, *Surface and Coatings Technology* **108–109**, 36 (1998).
18. J. A. Haynes, M. K. Ferber, W. D. Porter and E. D. Rigney, *Oxidation of Metals* **52**, 31 (1999).
19. W. J. Quadakkers, *Werkstoffe und Korrosion* **41**, 659–668 (1990).
20. P. Niranatlumpong, C. B. Ponton and H. E. Evans, *Oxidation of Metals* **53**, 241–258 (2000).
21. K. S. Ravichandran and K. An, *Journal of American Ceramic Society* **82**, 673 (1999).
22. K. An, K. S. Ravichandran, R. E. Dutton and S. L. Semiatin, *Journal of the American Ceramic Society* **82**, 399 (1999).
23. R. W. Trice, Y. J. Su, K. T. Faber, H. Wang and W. Porter, *Material and Science Engineering A* **272**, 284 (1999).
24. J. Bodzenta, *Chaos, Solitons and Fractals* **10**, 2087 (1999).
25. P. A. Medwick, H. E. Fischer and R. O. Pohl, *Journal of Alloys and Compounds* **203**, 67 (1994).
26. R. A. Miller, J. L. Smialek and R. G. Garlick, in *Advances in Ceramics 3: Science and Technology of Zirconia*, A. H. Heuer and L. W. Hobbs, eds. (American Ceramic Society, Columbus, OH, 1981) pp. 241–253.
27. L. Sagalowicz, P. Muralt, S. Hiboux, T. Maeder, K. Brooks, Z. Highelman and N. Setter, *Materials Research Society of Symposium Proceedings* **596**, 265 (2000).
28. S. L. Shinde, D. A. Olson, L. C. De Jonghe and R. A. Miller, *Ceramic Engineering Science Proceedings* **7**, 1032 (1986).
29. G. Muller, G. Schumacher and D. Straub, *Surface and Coatings Technology* **108–109**, 43 (1998).
30. N. Birks and G. H. Meier, *Introduction to High-temperature Oxidation of Metals* (Edward Arnold, London, 1983).
31. W. J. Brindley and R. A. Miller, *Surface and Coatings Technology* **43–44**, 446 (1990).